JACS
JOURNAL OF THE AMERICAN CHEMICAL SOCIETY
Article
pubs.acs.org/JACS

# A Fluorescence Light-Up Ag Nanocluster Probe That Discriminates Single-Nucleotide Variants by Emission Color

Hsin-Chih Yeh,*[,†,#] Jaswinder Sharma,[†] Ie-Ming Shih,[‡] Dung M. Vu,[§] Jennifer S. Martinez,*[,†] and James H. Werner*[,†]

[†]Center of Integrated Nanotechnologies, Los Alamos National Laboratory, Mail Stop K771, Los Alamos, New Mexico 87545, United States

[‡]Department of Pathology, School of Medicine, Johns Hopkins University, 1550 Orleans Street, Baltimore, Maryland 21231, United States

[§]Physical Chemistry & Applied Spectroscopy, Chemistry Division, Los Alamos National Laboratory, Mail Stop J567, Los Alamos, New Mexico 87545, United States

Supporting Information

**ABSTRACT:** Rapid and precise screening of small genetic variations, such as single-nucleotide polymorphisms (SNPs), among an individual's genome is still an unmet challenge at point-of-care settings. One crucial step toward this goal is the development of discrimination probes that require no enzymatic reaction and are easy to use. Here we report a new type of fluorescent molecular probe, termed a chameleon NanoCluster Beacon (cNCB), that lights up into different colors upon binding SNP targets. NanoCluster Beacons (NCBs) are collections of a small number of Ag atoms templated on single-stranded DNA that fluoresce strongly when placed in proximity to particular DNA sequences, termed enhancers. Here we show the fluorescence emission color of a NCB can change substantially (a shift of 60−70 nm in the emission maximum) depending upon the alignment between the silver nanocluster and the DNA enhancer sequence. Chameleon NCBs exploit this color shift to directly detect SNPs, based on the fact that different SNPs produce a different alignment between the Ag nanocluster and the enhancer. This SNP detection method has been validated on all single-nucleotide substitution scenarios in three synthetic DNA targets, in six disease-related SNP targets, and in two clinical samples taken from patients with ovarian serous borderline tumors. Samples with single-nucleotide variations can be easily identified by the naked eye under UV excitation, making this method a reliable and low-cost assay with a simple readout format.

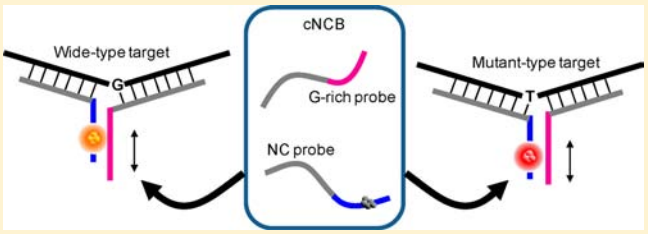


## INTRODUCTION

Single-nucleotide variations, such as single-nucleotide polymorphisms (SNPs)[1] or point mutations,[2] play an important role in many human diseases. As genetic markers, SNPs can be used to trace generational inheritance patterns associated with specific diseases. As diagnostic markers, point mutations can be used for early cancer detection.[3] Current methods for single-nucleotide variation detection (e.g., genotyping of known SNPs) typically require enzymatic reactions such as primer extension, ligation, and cleavage, making these methods time-consuming and expensive.[1] Hybridization-based methods, where discrimination readout can be optical,[4−8] electrical,[9,10] or electrochemical[11,12] signals, are considerably simpler in practice. However, most of these methods rely on differences in the free energy of probe/target binding for SNP differentiation (i.e., hybridization probes bind preferably the fully matched target rather than the single-base mismatched targets, such as molecular beacons[5,13]). Such differences in binding free energy are often small and can vary significantly on the basis of target sequence. Therefore, sophisticated probe design algorithms and use of hybridization enhancing moieties[14] are often necessary. Further, optimized assay conditions (such as elevated temperature for molecular beacon discrimination[13]) are often required, which also limit their use at point-of-care settings.

In addition to the methods mentioned above, new methods are being developed for SNP detection that do not rely on small differences in the free energy of probe/target binding for discrimination. For instance, SNPs have been detected by charge transport through the $\pi$-stack of DNA duplexes,[11,12] base-discriminating fluorescent nucleosides,[15,16] and kinetic schemes.[17,18] While overcoming the issue of small differences in binding free energy, these methods still produce on/off sensors that only differentiate a fully matched target from mismatched targets. Ideally, one would like to have a probe that can differentiate all four single-nucleotide variants (A, C, G, and T) at once and can quantify the amount of target present. Here we describe new molecular probes that display three different

Received: March 20, 2012
Published: July 10, 2012

   dx.doi.org/10.1021/ja3024737 | J. Am. Chem. Soc. 2012, 134, 11550−11558

colors when they bind four SNP targets. Moreover, these probes enable a two-dimensional analysis, where the fluorescence intensity quantitates the presence of nucleic acid targets and the fluorescence color identifies the single-nucleotide variants.

Our new probes use silver nanoclusters as fluorescence reporters[19−25] and build upon our recent discovery of a nanocluster light-up phenomenon.[26] Silver nanoclusters (collections of ∼2 to 30 silver atoms) are emerging fluorophores with many attractive features (e.g., subnanometer size, good brightness, and good photostability[20,27,28]) and useful properties (e.g., chemiluminescence[29] and electroluminescence[30]). Of particular importance for DNA detection and identification is the discovery that certain nonemissive DNA-templated silver nanoclusters (DNA/Ag NCs) can light up into distinct colors through interactions with different enhancer sequences.[26,31] On the basis of this finding, we designed molecular probes, termed NanoCluster Beacons (NCBs), which fluoresce upon binding specific DNA targets. Here we show an entirely new phenomenon—the color of the Ag NC can change substantially depending upon its position relative to an enhancer sequence. Furthermore, we exploit this new property for the sensitive detection and identification of a number of disease-related SNPs. We have termed these color-switching sensors of SNPs chameleon NanoCluster Beacons, cNCBs (Figure 1). Chameleon NanoCluster Beacons are easy to design, prepare, and use, thus providing a ready means for genotyping amplified DNA samples.

## EXPERIMENTAL SECTION

**Preparation of Silver Nanoclusters on DNA.** All DNA strands were purchased from Integrated DNA Technologies Incorporated and were purified by desalting. DNA/Ag NCs were made using the protocol developed by Petty and co-workers.[32] NC-bearing strands/NC probes were first dissolved in ultrapure deionized water. Ag NCs were formed by adding $AgNO_3$ (99.9%, Sigma-Aldrich) to the DNA solution, followed by reduction with $NaBH_4$. Final concentrations were 15 $\mu$M in NC-bearing strand, 180 $\mu$M in $AgNO_3$, and 180 $\mu$M in $NaBH_4$ in 20 mM pH 6.6 sodium phosphate buffer. The aqueous solution of $NaBH_4$ was prepared by dissolving $NaBH_4$ powder in water and adding the required volume to the DNA/$Ag^+$ mixture within 30 s, followed by vigorous shaking for 5 s. The reaction was kept in the dark at room temperature for 18 h before use. Probe-target hybridization was also carried out in 20 mM pH 6.6 sodium phosphate buffer at a 1:1 probe/target ratio. The sample was heated to 95 °C for 45 s and then slowly cooled to and kept at room temperature for 1 h.

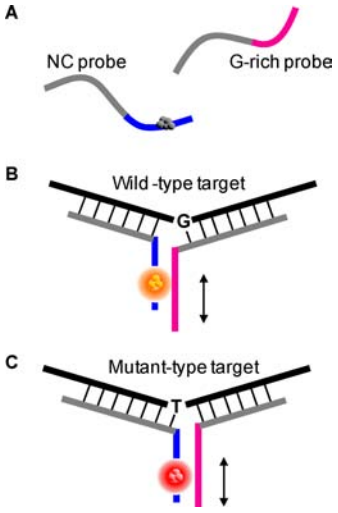


**Figure 1.** Chameleon NanoCluster Beacon (cNCB, which consists of a NC probe and a G-rich probe) lights up into different colors upon binding SNP targets. (A) Probes remain dark in the absence of targets. (B) Upon binding the wild-type target, the cNCB probe lights up into one color (in this example, orange). (C) Upon binding the mutant-type of target, the cNCB lights up into another color (in this example, red). The difference between wild-type and mutant-type targets is a single-nucleotide substitution (in this example, the G↔T substitution).

**Fluorescence Measurements.** Fluorescence was measured using a Varian Cary Eclipse fluorescence spectrophotometer. To eliminate the second order diffraction peak of the excitation source in the emission spectrum scan, a long pass filter (FF01-409/LP, Semrock) was placed in the emission light path. Absorbance was measured using an Agilent 8453 UV−vis spectrophotometer. The cuvette had 1 cm path length (16.100F-Q-10/z15, Starna Cells). Images of samples were acquired by a digital camera (Model no. C-770 ultra zoom, Olympus) with the samples illuminated by 365 nm light provided by a Syngene InGenius gel imager.

**Preparation of Clinical Samples.** Clinical specimens were prepared in the Department of Pathology at the Johns Hopkins Hospital, using a standard DNA extraction kit, QIAamp DNA Micro Kit, from Qiagen. The mutation status of *Kras* in two ovarian serous borderline tumors (SBTs) were validated by Sanger sequencing analysis using an ABI sequencer. One sample contained GGT→GAT mis-sense mutation at codon 12 (a heterozygous sample), and the other contained only wild-type *Kras* gene (a homozygous sample). Polymerase chain reaction was carried out using Taq polymerase and PCR buffers from New England BioLabs. The PCR products were purified using StrataClean resin from Agilent Technologies and then dialyzed in 400 mM pH 6.6 sodium phosphate buffer for 1 day and then dialyzed in deionized water for 3 days (a 5-L water bath was refreshed daily). The dialyzed PCR products were dehydrated using a speed-vac centrifuge and resuspended in 20 mM pH 6.6 sodium phosphate buffer, before mixing them with cNCB_3 (strands 52 and 53 in Table S1).

## RESULTS AND DISCUSSION

Here we show that different light-up colors can be obtained from the same NC-nucleation sequence (which carries a nonemissive Ag NC) and the same enhancer sequence by changing the position of the enhancer relative to the NC-nucleation sequence. As shown in Figure 2A and Figure S1, 11 different relative positions between the enhancer and the NC-nucleation sequences (named "position −3" to "position +7") were produced by hybridizing a common NC-bearing strand (strand 1 in Table S1, which carried nonemissive Ag NC) with 11 different guanine-rich (G-rich) strands (strands 2−12 in Table S1, which had a common enhancer sequence). The longest G-rich strand (G-rich strand "-3") contained 51 bases, with each subsequent G-rich strand shortened by one nucleotide. The 2D fluorescence contour plots (Figure 2B) show the hybridized samples generated multiple spectral peaks when excited in the visible to near-infrared region (450−800 nm). Corresponding to different light-up nanocluster species, these spectral peaks (called visible excitation peaks) could be categorized into four groups (Figure S4). Other than visible excitation peaks, UV excitation peaks appeared in the UV excitation region (250−400 nm, shown in the lower portion of the 2D plots with an independent intensity scale). We note that Fygenson and co-workers have recently explored the UV excitation of DNA/Ag NCs and assigned the UV excitation peaks as being due to absorption by DNA bases.[33] In dilute solutions, the UV excitation spectra of DNA/Ag NCs are well-


dx.doi.org/10.1021/ja3024737 | J. Am. Chem. Soc. 2012, 134, 11550−11558

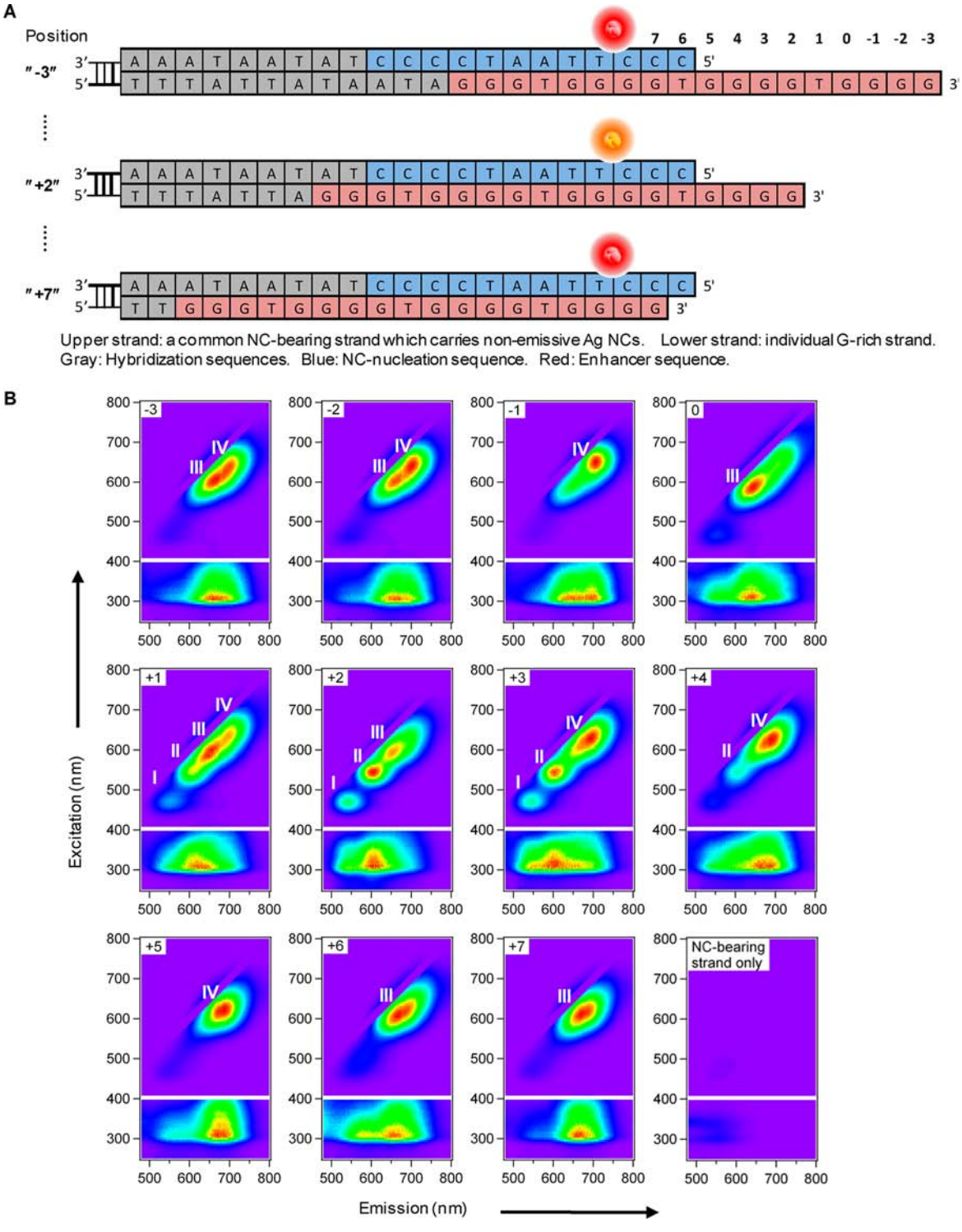


**Figure 2.** Eleven hybridized samples were prepared to investigate the effect of repositioning of the enhancer sequence with respect to the NC-nucleation sequence. These 11 samples consisted of a common NC-bearing strand (strand 1 in Table S1) and one of the 11 G-rich strands (strands 2−12), which differed by advancement of the enhancer sequence along the NC-nucleation sequence one nucleotide at a time, creating 11 relative positions between the enhancer and the NC-nucleation sequences. (A) Schematic shows three relative positions (**−3**, **+2**, and **+7**) between the enhancer sequence (red fill) and the NC-nucleation sequence (blue fill) (Figure S1, schematic of all 11 positions). A cartoon of a Ag NC is shown for positions **−3**, **+2**, and **+7**, which results in a red light-up color for positions **−3** and **+7** and a yellow/orange color for position **+2**. (B) 2D Fluorescence contour plots of the 11 hybridized samples and a control sample having only the NC-bearing strand, with the corresponding position number shown on the upper left corner of each plot. Twenty-one visible excitation peaks were found in the visible to near-infrared excitation region (450−800 nm), which were categorized into four groups (I, II, III, and IV, as indicated on the plots) based on their centroid locations.[34] The control sample (NC-bearing strand without a hybridization partner) showed little fluorescence. The UV excitation regions (250−400 nm, shown on the lower portion of the 2D plots) are independently scaled in order to better display the UV excitation peaks. The profiles of UV excitation peaks are different from those of visible excitation peaks (Figure S8).


dx.doi.org/10.1021/ja3024737 | J. Am. Chem. Soc. 2012, 134, 11550−11558

matched to absorption spectra of DNA (using short path length cuvettes).[33] Moreover, the fluorescence emission of DNA/Ag NCs upon UV excitation is highly depolarized, suggesting a rapid energy transfer mechanism between the bases and the Ag NCs.[33] Here, a similar mechanism is most likely responsible for the UV excitation features that we observed (Figures 2B and S6), albeit the UV excitation maxima in our spectra (ca. 300 nm) are red-shifted from the absorption maxima of the bases (ca. 260 nm). This red shift is due to the strong absorption of 260 nm light by the DNA bases. The 260 nm light is heavily attenuated by the time it reaches the center of the 1 cm cuvette (see Figure S6 for additional data and further discussion). Having similar UV excitation peaks for all Ag nanocluster species templated on DNA (regardless of their emission color)[19,32,33] is a useful feature for either multiplexed assays or homogeneous assays that employ a broad spectrum of fluorescent nanoclusters.

Due to these UV excitation peaks, bright colors of DNA/Ag NCs can be seen under UV light (Figure 3A). Visible excitation peaks were well resolved, symmetric, and distributed diagonally in the 2D fluorescence contour plots, whereas the UV excitation peaks were poorly resolved, asymmetric, and distributed horizontally (Figure S8). Despite these differences, the profiles of the UV excitation spectra reflect, to some extent, the types and the relative populations of light-up nanocluster species produced in individual samples. As a result, differences in the fluorescence emission color can be visualized among the 11 samples under UV 365 nm excitation (Figure 3A). The color variation is more clearly seen in Figure 3B, where the emission spectra are plotted. We used the emission-spectrum-global-maximum (ESGM, defined as the wavelength where the emission spectrum is the highest) as a gross indicator of color for each sample (Figure 3C). While we did not know the exact separation distance between the Ag NC and the enhancer sequence in each position, we found subtle repositioning of the enhancer sequence relative to the NC-nucleation sequence (e.g., from position **−1** to **0** or from position **+3** to **+4**) can shift the ESGM by as much as 60−70 nm (Figure 3C). The ability to obtain measurably different ensemble light-up colors using the same enhancer sequence shifted only by a single nucleotide is unique to NCBs. It is an environmental sensitivity not seen in organic dyes or semiconductor quantum dots that opens the door to the creation of a new type of molecular probe that can sense small variations in DNA sequences.

Why can the ESGM shift as much as 60−70 nm when the enhancer sequence is repositioned relative to the NC-nucleation sequence by a single nucleotide? Previously, we observed substantial green fluorescence enhancement on the same NC-nucleation sequence (which carried a nonemissive Ag NC) when an enhancer of 12 thymine bases (3′-$T_{12}$) was placed in proximity to the NC-nucleation sequence, whereas red fluorescence enhancement dominated for an enhancer of substantial guanine content (3′-$(G_4T)_3G_3$, which is also the enhancer sequence used in the position-shifting experiments shown in Figures 2 and 3).[26] These two different fluorescence emission colors from two distinct enhancer sequences demonstrated that the ligand/base environment surrounding the Ag NC is a strong determinant of the fluorescence emission color and intensity. One may argue that the red fluorescence emission from the G-rich enhancer is due to electron transfer from guanines to the Ag NC. In our previous investigations, we tested an enhancer where all guanines were replaced with 7-deazaguanines.[26] This enhancer failed to enhance the red

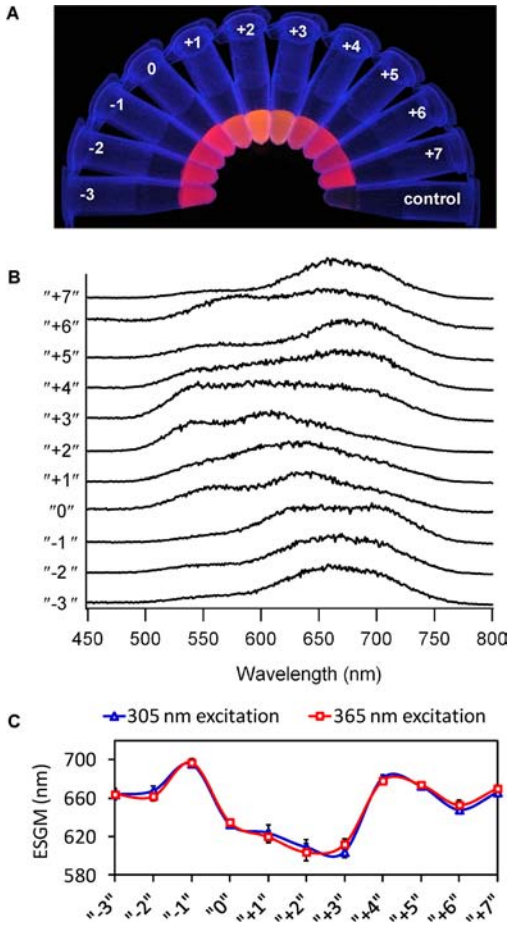


**Figure 3.** The light-up color of NanoCluster Beacons can be tuned by repositioning the enhancer sequence with respect to the NC-nucleation sequence. (A) Color photo of the 11 hybridized samples (position **−3** to **+7**) and the control sample (NC-bearing strand without a hybridization partner) under UV 365 nm light. The colors of position **+1**, **+2**, and **+3** samples were blue-shifted, mainly due to the presence of type I and type II light-up nanocluster species in these samples. The samples were in 1.5 mL Eppendorf tubes and were placed on a commercial gel imager. The image was acquired by a digital camera and presented here without any contrast/color adjustment. (B) Emission spectra of the 11 samples under 365 nm excitation (see Figure S5 for the absorption and circular dichroism spectra of these samples). (C) Emission-spectrum-global-maximum (ESGM) shifts substantially for the 11 hybridized samples and sets a simple criterion for color-switching probe design. Error bars represent the standard deviations of measurements taken from five independently prepared sample sets.

fluorescence of DNA/Ag NCs. This result significantly weakened the electron transfer hypothesis, as 7-deazaguanine is a stronger electron donor than guanine.[35] The only difference between guanine and 7-deazaguanine is that the N7 nitrogen atom is replaced by a carbon atom. A Fourier transform infrared spectroscopy study has shown that the N7 atom is the most preferable binding site for Ag ions.[36] Perhaps it is not surprising that deleting such an important interaction site in the ligand environment kills the red fluorescence enhancement. In addition, recent time-dependent density functional calculations on DNA/Ag NCs also indicated that the presence of low-energy electronic transitions strongly depends upon the ligand/base environment.[37] While we found a strong red fluorescence emission (emission maximum at 636 nm) emanated from a


dx.doi.org/10.1021/ja3024737 | J. Am. Chem. Soc. 2012, 134, 11550−11558

nearly poly-G enhancer and green emission (emission maximum at 535 nm) emanated from a poly-T enhancer,[26] we were curious what would happen for a heteropolymer enhancer with periodic $T_2$ and $G_2$ content (3′-$(T_2G_2)_4T_2$). We found, depending upon the relative position between the NC-nucleation and the heteropolymer enhancer sequences, that we could cycle the emission between green and red (Figure 4B).

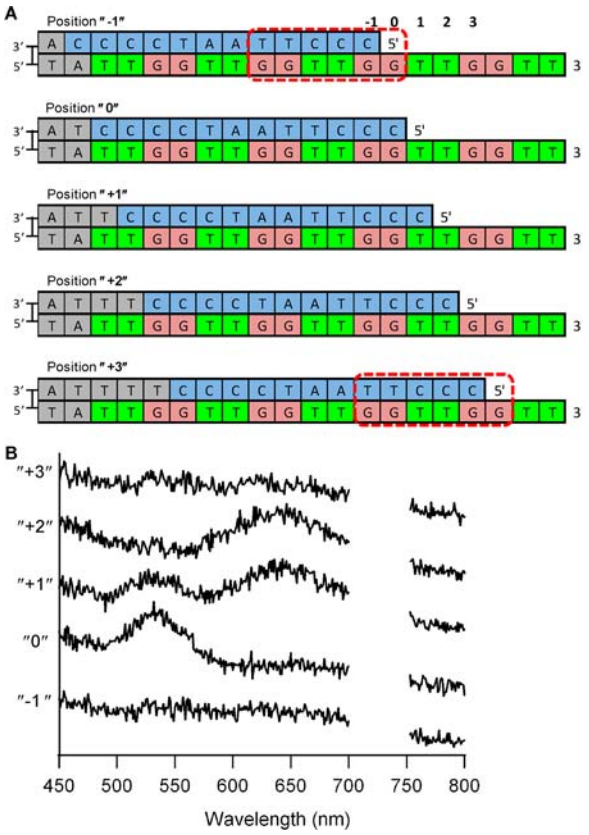


**Figure 4.** Five hybridized samples were prepared to investigate the mechanism underlying the observed repositioning-induced-color-tuning phenomenon. The 5 hybridized samples shown here consisted of a common heteropolymer enhancer strand (strand 54) and one of the 5 NC-bearing strands (strand 55 to 59) which differed by advancement of the NC-nucleation sequence along the enhancer sequence one nucleotide at a time, creating 5 relative positions between the enhancer and the NC-nucleation sequences. (A) Schematic shows all 5 relative positions (**−1** to **+3**) between the enhancer sequence (green/red fill) and the NC-nucleation sequence (blue fill). Assuming perfect alignment between the NC-nucleation sequences and the enhancer sequence, the ligand/base environment created around the TTCCC-5′ section of the NC-nucleation sequence is identical for positions **−1** and **+3**, as indicated by red boxes. (B) Fluorescence emission spectra of the 5 hybridized samples under 365 nm excitation. The spectra between 700−750 nm was removed due to a large peak caused by second-order diffraction of the 365 nm excitation.

Color switching between green and red suggests that a very short-range interaction (potentially direct contact) between the enhancer bases and the Ag NC determines the emission color of Ag NC. Due to this short-range interaction, it is not surprising that Figure 4B shows a 100 nm shift in ESGM from position **0** to position **+1**, corresponding to the spectral separation between the green (535 nm) and red (636 nm) light-up nanocluster species previously identified.[26]

While the light-up nanocluster species generated in Figure 2 (which have multiple spectral maxima) most likely represent an ensemble of several different nanocluster species, repositioning by two nucleotides from position **−1** to **+1** results in a substantial fraction of the nanocluster population being "greener". We hypothesize that in this situation, the nanocluster population in the position **+1** sample has more clusters in contact with a thymine base than clusters in position **−1** sample. We emphasize that Figures 2A, 4A and S1 are schematics to guide potential understanding, which may not reflect the true alignment between the NC-nucleation sequence and the enhancer sequence.

While a more precise understanding of the physical mechanism behind the ESGM shifts awaits a better determination of exact nanocluster sizes and positions on the DNA strand, here we exploit the large ESGM shifts seen upon a change in alignment by two nucleotides to directly and quantitatively identify SNPs. Our color-switching probes are based on a three-way-junction (3WJ) design[38] where a single-nucleotide substitution on the target DNA (positioned at the branch point of the 3WJ) causes frame-shift basepairing in the third arm (in our case, the nanocluster arm). This frame-shift basepairing moves the enhancer sequence relative to the NC-nucleation sequence by two nucleotides, resulting in different light-up colors.

As shown in Figure 5A, two positions (position **−1** and position **+1**) were generated by mixing cNCB_1 (strands 13 and 15 in Table S1) with *Kras* mutant-type target (sample **A**) and wild-type target (sample **B**). As predicted in the dsDNA system (Figure 2 and 3), the light-up color for position **+1** sample (wild-type target) should appear more "yellow/orange" as compared to the color for position **−1** sample (mutant-type target). Although the position **+1** in the cNCB system may not be exactly identical to the position **+1** in the dsDNA system (considering one is a three-strand system and the other is a two-strand system), sample **B** (wild-type, position **+1**) did appear more orange than sample **A** (mutant-type, position **−1**) (Figure 5B). These same two targets (mutant-type and wild-type) were also discriminated with another cNCB (cNCB_2), which utilized positions **0** and **+2** for color-switching sensing (see Figure S9 for detailed discussion). In contrast to most of the discrimination probes used today, cNCBs bind both wild-type and mutant-type targets with equal affinity (Figure S10). It is the different light-up colors created by hybridization of cNCBs to wild-type and mutant-type targets that enable discrimination. We note that in addition to being able to detect SNPs on short synthetic DNA, cNCB also shows good detection results on longer (120 nt) DNA targets (Figure S11).

We tested cNCB_1 on all four single-nucleotide variants (A, C, G, and T). These four cases resulted in three distinguishable and reproducible emission spectra (Figures 5C, S12, and S13). We (H.-C.Y.) have previously used a three-way-junction design, combined with monitoring Cy5 blinking dynamics by fluorescence correlation spectroscopy, for single-nucleotide variation detection.[38] Using the blinking time as an indicator, we showed that 4 single-nucleotide variants gave 3 distinguishable blinking times,[38] which agrees well with the 3 distinguishable emission spectra that we obtained using the cNCB detection method. The Cy5 blinking detection method, however, requires advanced detection tools to measure the change of Cy5 blinking dynamics at microsecond time scale. While a distinguishable color for each nucleotide variant is the ultimate goal, the ability to differentiate the four single-


dx.doi.org/10.1021/ja3024737 | J. Am. Chem. Soc. 2012, 134, 11550−11558

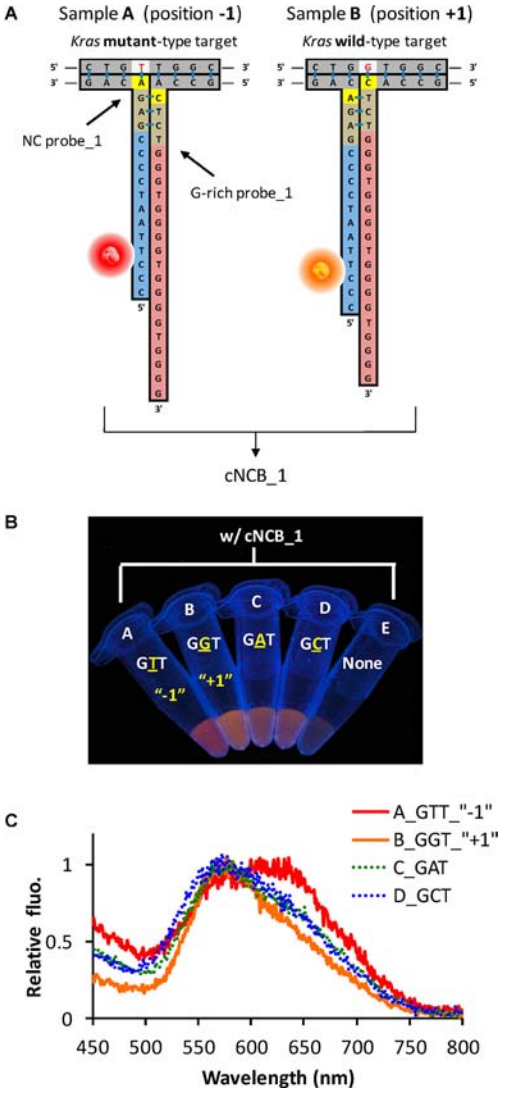


**Figure 5.** Schematic and results of a chameleon NanoCluster Beacon (cNCB_1) for single-nucleotide variation detection. cNCB_1, which was designed for *Kras* oncogene mutational analysis, consisted of G-rich probe_1 (strand 15 in Table S1) and NC probe_1 (strand 13). The single-nucleotide mutation under investigation is GGT (wild-type) to GTT (mutant-type) mutation on codon number 12.[40−42] (A) Schematic showing how different positions between the NC-nucleation sequence (blue fill) and the enhancer sequence (red fill) can be generated by mixing cNCB_1 with different targets. As illustrated, position **−1** (sample **A**) is generated by mixing cNCB_1 with *Kras* mutant-type target. However, if the thymine base on codon 12 (shown in red letter) is replaced by a guanine base, as shown on the wild-type target in sample **B**, frame-shift basepairing will lead to position **+1** after beacon/target hybridization. The structures of three-way junction shown here are schematics. The true structures may contain bulges (i.e., unpaired bases) at the branch points.[43] (B) Color photo of cNCB_1 mixing with all four SNP targets (**A**_GTT, **B**_GGT, **C**_GAT, and **D**_GCT) and the no-target control (**E**, having only cNCB_1) under 365 nm light. Sample **A** (position **−1**) was clearly the most red of the four, as predicted from Figure 3C. (C) Emission spectra of cNCB_1 mixing with the four SNP targets. Spectra were taken at 500 min after mixing (see Figure S12 for additional data and further discussion). These four samples resulted in three distinguishable emission spectra.

nucleotide variants into three groups still surpasses the state-of-the-art in SNP detection. Currently existing methods for SNP detection can only differentiate one matched target from three mismatched targets (i.e., only two different results for 4 different nucleotide variants).[4−17,39] Another important feature of cNCBs lies in their capability for a two-dimensional analysis. As shown in Figure 5B and further demonstrated in Figure S14, the fluorescence intensity can be used to check the existence of target or to quantify its amount, whereas fluorescence color (represented by the ESGM) identifies the type of target. Again, this feature is not shared by existing discrimination probes, where events without a target cannot be easily differentiated from events with a mismatched target (both give low fluorescence).

cNCB_1 and c_NCB_2 were specifically designed to differentiate one particular single-nucleotide substitution (G→T) at codon 12 of the *Kras* oncogene. We then endeavored to determine if *any* type of single-nucleotide substitution scenarios (G↔C, A↔T, T↔G, T↔C, G↔A, and A↔C) could be detected in this fashion. Three groups of targets (*Kras*, *Braf*, and sickle-cell anemia) were used to test all potential substitution scenarios. For each target, we created 4 NC probes and 4 G-rich probes (see Table S1), with a NC probe and G-rich probe pair defining a unique cNCB. Figure S15A, for instance, shows how *Kras*_NC probe_c and *Kras*_G-rich probe_g can be employed to differentiate G↔C single-nucleotide change. Twelve sample sets were prepared for each target group where each sample set used a unique cNCB. Each substitution scenario was tested with two cNCBs (for instance, sample set 1 and sample set 2 employed two different cNCBs but were both used to discriminate a C↔G substitution). As shown in Figure S15B, most of the 36 sample sets are differentiable under UV light, with the light-up color for those position **+1** samples (indicated on each sample tube) always appearing more yellow/orange. While examining the emission spectra of all sample sets under 365 nm excitation (Figure S15C), we found all six single-nucleotide substitution scenarios, for all three targets, could be differentiated with at least one cNCB.

To further demonstrate that cNCBs can be applied to detect a wide range of disease-related SNPs, we designed and tested cNCBs on six more SNP targets (such as SNPs associated with Werner's Syndrome and Type-2 Diabetes, see Table S3), which covered all six types of single-nucleotide substitution scenarios. We want to emphasize that the sequences around the SNP sites were not particularly chosen, and the design of cNCBs followed the examples given in Figure 6A. As shown in Figure 6B, cNCBs clearly differentiated the SNPs on all six targets, proving the general use of cNCBs.

In addition to the above characterization studies, we have successfully demonstrated the use of our cNCB to detect *Kras* point mutations in clinical samples. *Kras* mutations have been found in a variety of human neoplasms, including colorectal carcinoma and ovarian serous borderline tumors (SBTs). *Kras* mutations in SBTs often occur at codon 12,[40−42] which result in amino acid alterations and constitutive activation of this oncogene. Figure 7 shows a cNCB can successfully differentiate the GGT→GAT mutation at codon 12 for samples taken from patients with SBTs.

Chameleon NanoCluster Beacons represent a new class of hybridization-based discrimination probes that have many advantages over existing technologies, such as displaying three different colors among the four single-nucleotide variants (Figure 5C) and allowing for a two-dimensional analysis (Figure S14). Unlike most of the discrimination probes that


dx.doi.org/10.1021/ja3024737 | J. Am. Chem. Soc. 2012, 134, 11550−11558

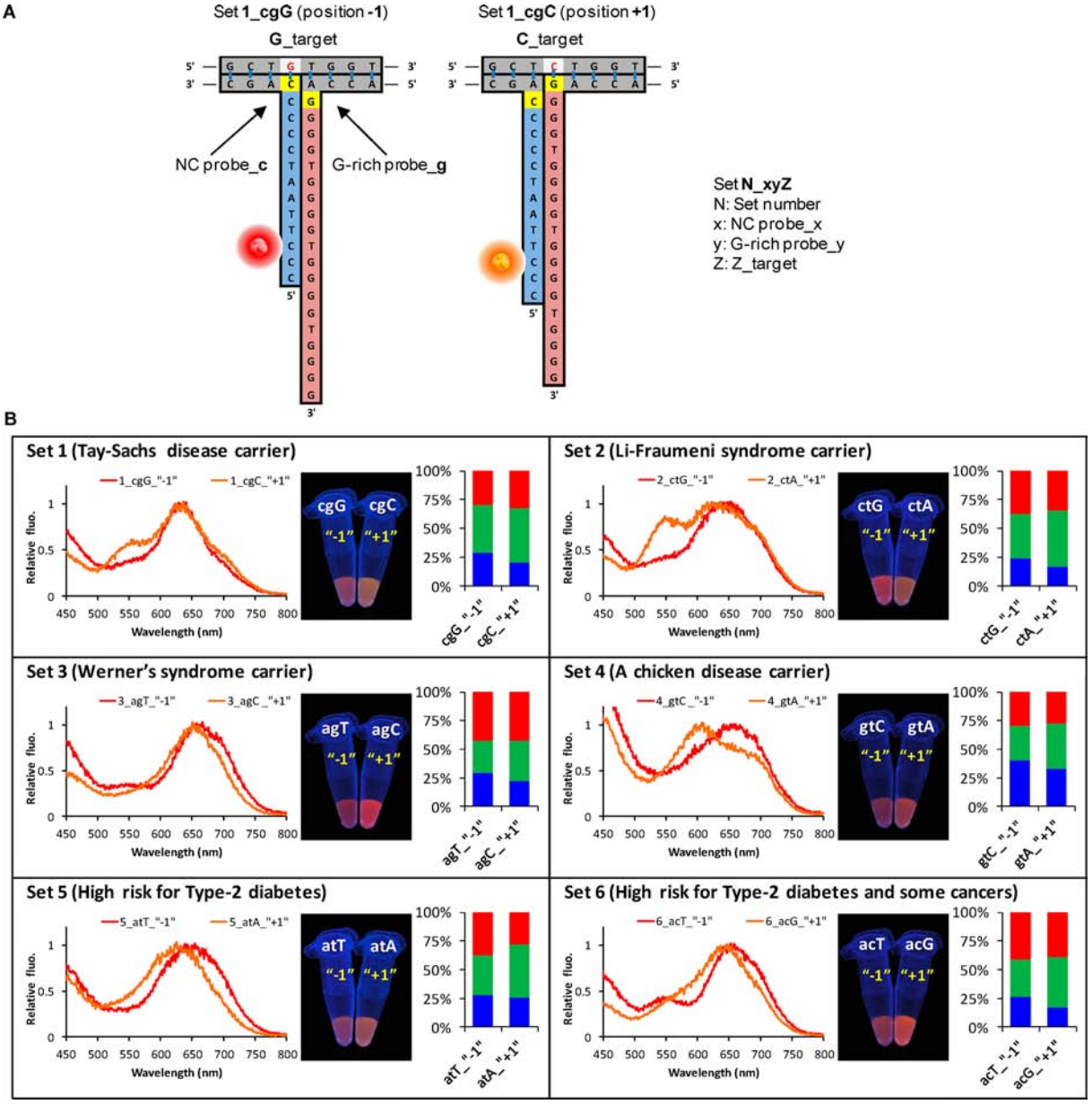


**Figure 6.** cNCBs can be generally applied to detect a wide variety of disease-related SNPs. We designed and tested cNCBs on 6 SNP targets (see Table S3 for the list of probes and targets), which covered all 6 types of single-nucleotide substitution scenarios (C→G: Set 1, G→A: Set 2, C→T: Set 3, A→C: Set 4, T→A: Set 5, and G→T: Set 6). We emphasize that the sequences around the SNP sites were not particularly chosen. (A) Design of cNCBs and nomenclature of the samples. (B) Detection results of the 6 cNCBs. As expected, all SNP targets were clearly differentiated based on their emission spectra (for position **+1** samples always being blue-shifted), proving the general use of cNCBs. The integrated emission spectrum from 420 to 800 nm (normalized to unity) was divided into three elements: blue, 420−510 nm; green, 510−640 nm; and red, 640−800 nm. The percentiles of the 3 color elements in each detection sample are shown in the stacked columns on the right, serving as a simple criterion for SNP scoring.

rely on differences in probe/target binding free energy for single-nucleotide differentiation (e.g., molecular beacons[5,13]), cNCBs work at room temperature and are easy to design/optimize. We note there are other DNA probes that can differentiate SNPs without relying on differences in probe/target binding affinities, such base-discriminating fluorescent (BDF) nucleosides.[16] However, BDF nucleosides rely on fluorescence intensity for discrimination and sometimes the differences in intensity from matched targets and mismatched targets are less than 2-fold. We point out that DNA/Ag NCs were previously used for SNP detection by Wang and co-workers.[39] Their method utilized hybridized DNA structures with a six-cytosine loop as templates for Ag NC synthesis and reported single-nucleotide variation detection.[39] As with BDF probes, Wang's method differentiates variants by the level of fluorescence intensity. It required Ag NCs to be synthesized after probe/target hybridization, leading to a longer assay time. Moreover, it is not clear whether or not such a method can be used to discriminate a wide variety of SNP targets. On the other hand, our probes have been validated on a large number of SNP targets and are straightforward to design and prepare. Unlike methods that require electrochemical detection,[11,12] atomic force microscopy,[17] or a gel shift assay,[18] identification of samples by color switching can be unambiguously carried out


dx.doi.org/10.1021/ja3024737 | J. Am. Chem. Soc. 2012, 134, 11550−11558

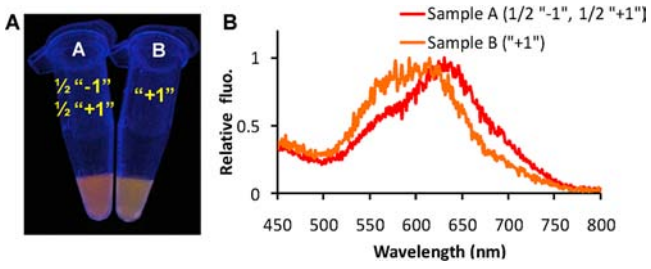


**Figure 7.** Detection of *Kras* point mutations in two clinical samples using a cNCB. Sample **A** contained *Kras* heterozygous targets (both GGT and GAT targets), while sample **B** contained only *Kras* wild-type target (GGT target). The cNCB used here (denoted cNCB_3) consisted of NC probe_3 and G-rich probe_3 (strands 52 and 53 in Table S1), which was designed to generate position **+1** with the GGT target and position **−1** with the GAT target. (A) Color photo of cNCB_3 mixing with DNA amplified from the two clinical samples (see Experimental Section for sample preparation). The color of sample **A** (with both GGT and GAT targets) clearly appeared red-shifted due to the fact that about half of its targets generated position **−1** when hybridized with cNCB_3. (B) Emission spectra of samples **A** and **B**.

by the naked eye under UV excitation, making cNCBs easy to use at point-of-care settings. Moreover, we point out our SNP detection scheme is fully compatible with microarray technologies for high throughput analysis.

## CONCLUSION

We have found that the ESGM of an ensemble of DNA/Ag NCs can shift as much as 60−70 nm due to a subtle change in alignment between the NC-nucleation sequence and the enhancer sequence. It is this environmental sensitivity that lays the foundation of our signal-based amplification detection scheme.[44] Combining this repositioning-induced-color-tuning property with a three-way junction design,[38] we have created cNCBs that can be used to quantify and identify SNPs in a light-up, color-switching fashion. Here we demonstrate the use of cNCBs in the direct discrimination of 6 disease-related SNPs and also on DNA amplified directly from clinical samples of ovarian SBTs. The common UV excitation feature of all DNA/Ag NCs allows a single excitation source to be used to simultaneously excite all DNA/Ag NCs present in the population,[19,32,33] greatly simplifying the instrumentation needed for field-based diagnostics.

We have hypothesized that the different light-up colors are due to different ligand/base environments around the Ag NCs, with greener cluster ensembles having more thymine bases in contact with the Ag NCs. A better understanding should grow from concerted efforts to map out the relationship between fluorescence emission and (i) atom number in the cluster, (ii) template conformation, (iii) cluster charge state, and (iv) detailed cluster-base binding geometry.

In addition to SNP discrimination, the environmental sensitivity of DNA/Ag NCs could also be used to create a spectroscopic ruler that can report small conformational changes or changes in spatial arrangement due to various biomolecular interactions. Such a ruler would complement existing spectroscopic rulers, such energy transfer-based,[45] electron transfer-based,[46] switching dynamics-based,[47] nano-metal surface energy transfer-based,[48] or plasmon coupling-based rulers.[49]

## ASSOCIATED CONTENT

### Supporting Information

Description of the material included, results from other associated experiments, and further discussion of UV excitation spectra. This material is available free of charge via the Internet at http://pubs.acs.org.

## AUTHOR INFORMATION

### Corresponding Author

tim.yeh@austin.utexas.edu; jenm@lanl.gov; jwerner@lanl.gov

### Present Address

[#]Department of Biomedical Engineering, The University of Texas at Austin, Austin, Texas 78712, United States

### Notes

The authors declare no competing financial interest.

## ACKNOWLEDGMENTS

The authors thank L. Chen for many useful discussions and help in PCR. The authors also thank P.-E. Li for help in searching the SNP database and H.-L. Wang for help in melting temperature measurements. This work was supported through Los Alamos National Laboratory Directed Research and Development (LDRD) and was performed at the Center for Integrated Nanotechnologies, a U.S. Department of Energy, Office of Basic Energy Sciences user facility at Los Alamos National Laboratory (Contract DE-AC52-06NA25396). The work at Johns Hopkins Hospital was supported by NIH/NCI (CA129080 and CA103937) to I.-M.S.

## REFERENCES

(1) Kwok, P. Y. *Ann. Rev. Genomics Hum. Genetics* **2001**, *2*, 235.
(2) Tian, D. C.; Wang, Q.; Zhang, P. F.; Araki, H.; Yang, S. H.; Kreitman, M.; Nagylaki, T.; Hudson, R.; Bergelson, J.; Chen, J. Q. *Nature* **2008**, *455*, 105.
(3) Wilentz, R. E.; Chung, C. H.; Sturm, P. D. J.; Musler, A.; Sohn, T. A.; Offerhaus, G. J. A.; Yeo, C. J.; Hruban, R. H.; Slebos, R. J. C. *Cancer* **1998**, *82*, 96.
(4) Wang, D. G.; Fan, J. B.; Siao, C. J.; Berno, A.; Young, P.; Sapolsky, R.; Ghandour, G.; Perkins, N.; Winchester, E.; Spencer, J.; Kruglyak, L.; Stein, L.; Hsie, L.; Topaloglou, T.; Hubbell, E.; Robinson, E.; Mittmann, M.; Morris, M. S.; Shen, N. P.; Kilburn, D.; Rioux, J.; Nusbaum, C.; Rozen, S.; Hudson, T. J.; Lipshutz, R.; Chee, M.; Lander, E. S. *Science* **1998**, *280*, 1077.
(5) Kostrikis, L. G.; Tyagi, S.; Mhlanga, M. M.; Ho, D. D.; Kramer, F. R. *Science* **1998**, *279*, 1228.
(6) Zhong, X. B.; Reynolds, R.; Kidd, J. R.; Kidd, K. K.; Jenison, R.; Marlar, R. A.; Ward, D. C. *Proc. Natl. Acad. Sci. U.S.A.* **2003**, *100*, 11559.
(7) Kolpashchikov, D. M. *J. Am. Chem. Soc.* **2005**, *127*, 12442.
(8) Xiao, Y.; Plakos, K. J. I.; Lou, X.; White, R. J.; Qian, J.; Plaxco, K. W.; Soh, H. T. *Angew. Chem., Int. Ed.* **2009**, *48*, 4354.
(9) Park, S. J.; Taton, T. A.; Mirkin, C. A. *Science* **2002**, *295*, 1503.
(10) Star, A.; Tu, E.; Niemann, J.; Gabriel, J. C. P.; Joiner, C. S.; Valcke, C. *Proc. Natl. Acad. Sci. U.S.A.* **2006**, *103*, 921.
(11) Boon, E. M.; Ceres, D. M.; Drummond, T. G.; Hill, M. G.; Barton, J. K. *Nat. Biotechnol.* **2000**, *18*, 1096.
(12) Inouye, M.; Ikeda, R.; Takase, M.; Tsuri, T.; Chiba, J. *Proc. Natl. Acad. Sci. U.S.A.* **2005**, *102*, 11606.
(13) Mhlanga, M. M.; Malmberg, L. *Methods* **2001**, *25*, 463.
(14) de Kok, J. B.; Wiegerinck, E. T. G.; Giesendorf, B. A. J.; Swinkels, D. W. *Hum. Mutation* **2002**, *19*, 554.
(15) Okamoto, A.; Kanatani, K.; Saito, I. *J. Am. Chem. Soc.* **2004**, *126*, 4820.
(16) Okamoto, A.; Saito, Y.; Saito, I. *J. Photochem. Photobiol., C* **2005**, *6*, 108.

(17) Subramanian, H. K. K.; Chakraborty, B.; Sha, R.; Seeman, N. C. *Nano Lett.* **2011**, *11*, 910.
(18) Buck, A. H.; Campbell, C. J.; Dickinson, P.; Mountford, C. P.; Stoquert, H. C.; Terry, J. G.; Evans, S. A. G.; Keane, L. M.; Su, T.-J.; Mount, A. R.; Walton, A. J.; Beattie, J. S.; Crain, J.; Ghazal, P. *Anal. Chem.* **2007**, *79*, 4724.
(19) Petty, J. T.; Zheng, J.; Hud, N. V.; Dickson, R. M. *J. Am. Chem. Soc.* **2004**, *126*, 5207.
(20) Vosch, T.; Antoku, Y.; Hsiang, J.-C.; Richards, C. I.; Gonzalez, J. I.; Dickson, R. M. *Proc. Natl. Acad. Sci. U.S.A.* **2007**, *104*, 12616.
(21) Gwinn, E. G.; O'Neill, P.; Guerrero, A. J.; Bouwmeester, D.; Fygenson, D. K. *Adv. Mater.* **2008**, *20*, 279.
(22) Petty, J. T.; Sengupta, B.; Story, S. P.; Degtyareva, N. N. *Anal. Chem.* **2011**, *83*, 5957.
(23) Sharma, J.; Yeh, H.-C.; Yoo, H.; Werner, J. H.; Martinez, J. S. *Chem. Commun.* **2010**, *46*, 3280.
(24) Sharma, J.; Yeh, H. C.; Yoo, H.; Werner, J. H.; Martinez, J. S. *Chem. Commun.* **2011**, *47*, 2294.
(25) Neidig, M. L.; Sharma, J.; Yeh, H.-C.; Martinez, J. S.; Conradson, S. D.; Shreve, A. P. *J. Am. Chem. Soc.* **2011**, *133*, 11837.
(26) Yeh, H.-C.; Sharma, J.; Han, J. J.; Martinez, J. S.; Werner, J. H. *Nano Lett.* **2010**, *10*, 3106.
(27) Diez, I.; Ras, R. H. A. *Nanoscale* **2011**, *3*, 1963.
(28) Xu, H. X.; Suslick, K. S. *Adv. Mater.* **2010**, *22*, 1078.
(29) Konig, L.; Rabin, I.; Schulze, W.; Ertl, G. *Science* **1996**, *274*, 1353.
(30) Lee, T. H.; Gonzalez, J. I.; Dickson, R. M. *Proc. Natl. Acad. Sci. U.S.A.* **2002**, *99*, 10272.
(31) Yeh, H.-C.; Sharma, J.; Han, J. J.; Martinez, J. S.; Werner, J. H. *IEEE Nanotechnol. Mag.* **2011**, *5*, 28.
(32) Ritchie, C. M.; Johnsen, K. R.; Kiser, J. R.; Antoku, Y.; Dickson, R. M.; Petty, J. T. *J. Phys. Chem. C* **2007**, *111*, 175.
(33) O'Neill, P. R.; Gwinn, E. G.; Fygenson, D. K. *J. Phys. Chem. C* **2011**, *115*, 24061.
(34) O'Neill, P. R.; Velazquez, L. R.; Dunn, D. G.; Gwinn, E. G.; Fygenson, D. K. *J. Phys. Chem. C* **2009**, *113*, 4229.
(35) Heinlein, T.; Knemeyer, J.-P.; Piestert, O.; Sauer, M. H. M. *J. Phys. Chem. B* **2003**, *107*, 7957.
(36) Arakawa, H.; Neault, J. F.; Tajmir-Riahi, H. A. *Biophys. J.* **2001**, *81*, 1580.
(37) Soto-Verdugo, V.; Metiu, H.; Gwinn, E. *J. Chem. Phys.* **2010**, *132*, 195102.
(38) Yeh, H.-C.; Puleo, C. M.; Ho, Y.-P.; Bailey, V. J.; Lim, T. C.; Liu, K.; Wang, T.-H. *Biophys. J.* **2008**, *95*, 729.
(39) Guo, W.; Yuan, J.; Dong, Q.; Wang, E. *J. Am. Chem. Soc.* **2009**, *132*, 932.
(40) Ho, C. L.; Karman, R. J.; Dehari, R.; Wang, T. L.; Shih, I. M. *Cancer Res.* **2004**, *64*, 6915.
(41) Kurman, R. J.; Shih, I. M. *Int. J. Gynecol. Pathol.* **2008**, *27*, 151.
(42) Yeh, H. C.; Ho, Y. P.; Shih, I. M.; Wang, T. H. *Nucleic Acids Res.* **2006**, *34*, e35.
(43) Lilley, D. M. J. *Q. Rev. Biophys.* **2000**, *33*, 109.
(44) Giljohann, D. A.; Mirkin, C. A. *Nature* **2009**, *462*, 461.
(45) Stryer, L.; Haugland, R. P. *Proc. Natl. Acad. Sci. U.S.A.* **1967**, *58*, 719.
(46) Yang, H.; Luo, G. B.; Karnchanaphanurach, P.; Louie, T. M.; Rech, I.; Cova, S.; Xun, L. Y.; Xie, X. S. *Science* **2003**, *302*, 262.
(47) Bates, M.; Blosser, T. R.; Zhuang, X. W. *Phys. Rev. Lett.* **2005**, *94*, 108101.
(48) Yun, C. S.; Javier, A.; Jennings, T.; Fisher, M.; Hira, S.; Peterson, S.; Hopkins, B.; Reich, N. O.; Strouse, G. F. *J. Am. Chem. Soc.* **2005**, *127*, 3115.
(49) Sonnichsen, C.; Reinhard, B. M.; Liphardt, J.; Alivisatos, A. P. *Nat. Biotechnol.* **2005**, *23*, 741.